Magnetic Resonance Compatibility of Multichannel Silicon Microelectrode Systems for Neural Recording and Stimulation: Design Criteria, Tests, and Recommendations

Francisco M. Martínez Santiesteban*, *Member, IEEE*, Scott D. Swanson, Douglas C. Noll, *Member, IEEE*, and David J. Anderson

***Abstract*—Magnetic resonance (MR) compatibility of biomedical implants and devices represents a challenge for designers and potential risks for users. This paper addresses these problems and presents the first MR-compatible multichannel silicon chronic microelectrode system, used for recording and electrical stimulation of the central nervous system for animal models. A standard chronic assembly, from the Center for Neural Communication Technology at the University of Michigan, was tested on a 2 Tesla magnet to detect forces, heating, and image distortions, and modified to minimize or eliminate susceptibility artifacts, tissue damage, and electrode displacement, maintaining good image quality and safety to the animals. Multiple commercial connectors were tested for MR compatibility and several options for the reference electrode were also tested to minimize image artifacts and provide a stable biocompatible reference for short- and long-term neural recordings. Different holding screws were tested to anchor the microelectrode assembly on the top of the skull. The final selection of this part was based on MR-compatibility, biocompatibility, durability, and mechanical and chemical stability. The required adaptor to interconnect the MR-compatible microelectrode with standard data acquisition systems was also designed and fabricated. The final design is fully MR-compatible and has been successfully tested on guinea pigs.**

***Index Terms*—Biomedical implants, magnetic resonance compatibility, magnetic resonance imaging, magnetic susceptibility, multichannel silicon microelectrodes.**

I. Introduction

BASED on the manipulation of strong magnetic fields and radio frequency (RF) signals, magnetic resonance imaging (MRI) is one of the most powerful imaging techniques used for research and clinical applications. Furthermore, during the last years functional MRI (fMRI) has shown its importance on the study of brain responses to different stimuli. Although highly safe, there are some minor, infrequent, and well-known biological effects related with MRI, such as peripheral nerve stimulation and retinal magnetic phosphene stimulation [1]. Until now, there is no evidence suggesting any concern with the use of MRI at magnetic flux densities up to 3 T. In the United States, the Food and Drug Administration (FDA) considers significant risk, for MR diagnostic devices, when the main static magnetic field is greater than 4 T, for infants aged 1 month or less, and greater than 8 T, for patients above 1 month of age [2], although at ultra-high magnetic flux densities (>8 T) more studies might be required [3].

In general, MRI is contraindicated on patients and individuals with non-MR compatible biomedical implants, unless very specific procedures are followed [1], [4], [5]. Some of the potential risks associated with MRI and biomedical implants include attraction, deflection, and displacement of implants, malfunction of electronically activated devices, and heating or burn of devices and tissue, all of them produced by the following interactions with the static or dynamic magnetic fields:

1) Forces and Torques: As comprehensively presented by Schenck, using simplified implant models and equations, translational and rotational forces acting on a biomedical implant depend on the shape, volume, and magnetic susceptibility of the object; its position and orientation with respect to the magnetic field; and magnetic field strength and type of magnet [6]. Shellock *et al.* present significant differences on the magnitude and location of these forces depending on the physical characteristics of the magnet, i.e., short- or long-bore, cylindrical or open magnets, and shielded or unshielded static magnetic fields, which defines the maximum spatial gradient of the magnetic field [7]–[9]. Furthermore, in the presence of electric and magnetic fields, ionic charges in fluids inside the body and electric currents flowing in circuits and leads of biomedical implants are subject to Lorentzian forces, which normally are very small [6].

Based on the specifications of the American Society of Testing and Materials (ASTM), a device is MR safe, for MR induced displacements, if the magnetically induced force is less than the weight of the object [10]. Similarly, if the product of the weight of the device and its longest dimension is less than the maximal MR induced torque, then the object could be considered MR safe, for magnetically induced rotational forces [11].

Manuscript received November 17, 2004; revised June 28, 2005. This work was supported by the University of Michigan Center for Neural Communication Technology. *Asterisk indicates corresponding author.*

*F. M. Martínez Santiesteban is with the Department of Biomedical Engineering, University of Michigan, 2231 Stone Road, Ann Arbor, MI 48109 USA (e-mail: sfmartin@umich.edu).

S. D. Swanson is with the Department of Radiology, University of Michigan, Ann Arbor, MI 48109 USA.

D. C. Noll is with the Department of Radiology and the Department of Biomedical Engineering, University of Michigan, Ann Arbor, MI 48109 USA.

D. J. Anderson is with the Departments of Biomedical Engineering, Otorhinolaryngology, and Electrical Engineering and Computer Science, University of Michigan, Ann Arbor, MI 48109 USA.

Digital Object Identifier 10.1109/TBME.2005.864497

2) Gradient Switching- and RF Pulses-Induced Heating: Temporal changing magnetic fields may induce electric currents, and intrinsically in MRI two changing magnetic fields are present: the relatively low frequency field created by the switching electric currents of the gradient coils, and the high frequency changing field of the RF signal, emitted by the transmitting coil or set of coils. The biological effects of changing magnetic fields are extensively discussed by Shellock and are not the focus of this paper [1]. What is relevant for this investigation are the induced voltage and possible induced Eddy currents created in the presence of conductive closed loops or volumes. For neural implants, the induced voltage and Eddy currents may produce signal artifacts, spurious stimulation, malfunction of electronic devices, MR signal loss, image distortion, and some degree of heating that normally is not capable of producing thermal injury, unless a resonant condition is achieved [12].

A specific type of current induction known as "antenna effect" occurs in open leads, entirely or fractionally inside the magnet, capable of producing severe burnings. The physical principles of this RF-induced heating and different strategies to minimize it have been analyzed and discussed elsewhere and are not covered on this work [12]–[20]. For our investigation, this condition may occur if the leads of the data acquisition system remain unconnected from the recording or stimulating channels. Normally, heating is confined to the ends of the wire and is maximized in a range of values around or near the resonant length, although extreme-heating conditions may occur even at significantly shorter lengths [17]. Besides heating, the antenna effect also creates localized variations on the applied RF signal, producing hot spots, distortions and ghosts that may affect the quality of the MR images [13], [21].

For MR induced heating, the FDA accepts a maximal whole body temperature increase of 1 °C, under medical supervision, and a maximal temperature of 38 °C, 39 °C, and 40 °C for localized heating in head, torso, and extremities, respectively [22], [23].

Given the seriousness of the mentioned potential risks and some reported accidents associated with MRI, scientists and organizations have placed significant efforts and resources to test medical devices and educate people working on MRI facilities [1], [3], [24]–[31]. Nevertheless, a worldwide regulation and standardization is still required [32].

3) Image Artifacts: Different studies have been conducted to evaluate and achieve the MR safety and MR compatibility of several biomedical implants. Normally, on those devices, ferromagnetic materials have been replaced with titanium, stainless-steel 300 series, or other nonmagnetic alloys such as Elgiloy, Phynox, or MP35N [4], [9], [33]. In some studies, wire leads have been replaced with fiber optic cable or carbon fiber conductors and some have reported the use of electrodes made of tungsten, tin, or carbon, all of them nonmagnetic [34]–[39]. Unfortunately, some of these devices present significant distortions on images and, although they may be considered MR safe, some cannot be classified as MR compatible.

The terms "MR Safe" and "MR Compatible" are often loosely used and improperly exchanged, and some MRI equipment manufacturers have their own classifications for different zones, depending to the closeness to the imaging region [40]. For the purpose of this paper, the definitions established by the ASTM will be used [10], [11], [41], [42]. They stipulate that, when used in MR environments, an "MR Safe" device does not present additional risk to patients or other individual but may affect the diagnostic information of the MR images, whereas and "MR Compatible" device is MR safe and the diagnostic information of the MR images and the operation of the device are not affected. For both definitions, it is important to specify the MR conditions that define the safety or compatibility of the device, e.g., magnetic field strength and type of magnet, because the object may not be safe or compatible under more extreme MR conditions.

As can be seen, image quality is associated with MR compatibility and, as comprehensively explained by Schenk, both are strongly correlated with the magnetic susceptibility differences $\Delta\chi = |\chi - \chi_{\mathrm{T}}|$ between an object (χ) and the surrounding tissue (χ_{T}) [43]. In general, $\Delta\chi \leq 10\ \mathrm{ppm}$ produces small to insignificant image artifacts, $10 < \Delta\chi \leq 200\ \mathrm{ppm}$ produces notorious and often detrimental image distortions, and $\Delta\chi > 200\ \mathrm{ppm}$ not only produces intolerable image distortions but also rotational and translational forces are evident and represent potential hazards. These observations are valid for conventional gradient echo (GE) or spin echo (SE) acquisition schemes, and exclude T_2^* weighted images obtained with fast pulse sequences, such as echo planar imaging (EPI). Those fast pulse sequences are very sensitive to magnetic susceptibility differences such as the present at the air-tissue interface $(\Delta\chi \approx 10\ \mathrm{ppm})$, which produces significant distortions, or between oxygenated and deoxygenated hemoglobin $(\Delta\chi \approx 2.26\ \mathrm{ppm})$, which generates the blood-oxygenation-level-dependant (BOLD) effect used to detect brain activation [44]. Table I presents some values of magnetic susceptibility properties of common materials associated with human tissue, recording electrodes, and electronic amplifiers used for neural recordings.

To the best of our knowledge, until now, there is no relevant information that relates MRI and silicon microelectrodes. Most of the studies involving microelectrodes in animal models are oriented to glass micropipettes or wire microelectrodes where the position of the implanted electrodes is commonly determined via postmortem techniques. For experiments where MRI is used, the magnetic susceptibility difference between the surrounding tissue and the metallic implant causes a significant signal loss around the electrode so that its position is evident and some image distortion around it is tolerated [51]. In some studies, a ferromagnetic material is electrochemically deposited in the tissue using a stainless-steel microelectrode. After the electrode is removed, high-resolution MR images show a small susceptibility distortion where the implant was located, but not so strong to significantly distort the images [52]. More recently, Shyu *et al.* presented important advantages of single-channel carbon fiber microelectrodes over wire microelectrodes for fMRI studies in rats [53]. Currently, for human studies, the electrodes are relatively large and contain metallic materials. Some can be used within MRI environments, although X-Ray or computed tomography (CT) are the preferred imaging technologies to determine their location since they present similar problems and potential risks for MRI as the observed with wire microelectrodes [54]–[56].

TABLE I
MAGNETIC SUSCEPTIBILITY OF COMMON MATERIALS ASSOCIATED WITH HUMAN TISSUE, ELECTROPHYSIOLOGICAL SIGNAL RECORDING ELECTRODES, AND ELECTRONIC DEVICES USED TO AMPLIFY NEURAL RECORDINGS. VALUES WERE OBTAINED FROM [43] UNLESS SPECIFIED. WHEN REQUIRED, MOLAR SUSCEPTIBILITY VALUES WERE CONVERTED TO THE STANDARD SI VOLUME SUSCEPTIBILITY. FOR INFORMATION ABOUT SILICON MICROELECTRODES COMPOSITION, SEE [45] AND [46]

MATERIAL	MAGNETIC SUSCEPTIBILITY χ (ppm)	COMMENT
Carbon	-204	High impedance conductors for simultaneous EEG/MRI.
Gold	-34	EEG surface electrodes, bonding pads of silicon microelectrodes.
Silver	-24	EEG surface electrodes, wires, electronic devices.
Tin	-23	Plating of connectors, wires, and leads of electronic devices.
Boron	-18.22 [47]	Silicon microelectrode substrate.
Silicon oxide	-16.3	Silicon microelectrode dielectric films.
Lead	-15.8	Batteries, printed circuit boards, electronic devices, soldering material.
Copper	-9.63	Wires, printed circuit boards, lead frame of electronic devices.
Human Tissue	-11.0 to -7.0	
Water (37 °C)	-9.05	
Silicon Nitride	-9.0	Silicon microelectrode dielectric films.
Cortical Bone	-8.86	
Deoxygenated Blood	-7.9	
Germanium	-7.1	Electronic devices.
Silicon	-4.2	Electronic devices, silicon microectrodes.
Air (NTP)	0.36	
Aluminum	20.7	Electronic devices, silicon microelectrode bonding wires.
Iridium	37.66 [47]	Wire microelectrodes.
Tungsten	77.2	Wire microelectrodes.
Iridium oxide	146.89 [48]-[49]	Recording and stimulating sites of silicon microelectrodes.
Tantalum	178	Electronic devices.
Titanium	182	Holding screws, reference electrodes, biomedical implants.
Platinum	279	Wire microelectrodes, biomedical implants.
Stainless Steel 316	9000 [50]	Surgical devices, biomedical implants.
Cobalt	250×10^6	Electronic devices.
Nickel	600×10^6	Plating in connectors and electronic devices.
Iron	200×10^9	Lead frame of electronic devices.

In this paper, we present a silicon-based microelectrode that, given its dimensions (3–10 mm length, 15 μm thick, 33–500 μm width, [57]) and low magnetic susceptibility signature, allows not only multichannel recordings or stimulation of the CNS in animal models, but also does not represent a risk in MRI environments and, more importantly, does not produce noticeable image distortions for *in vivo* studies using MRI.

II. METHODS

A. Initial Assessment

The standard chronic silicon microelectrodes (S−SiμE), presented in Fig. 1, was tested for MR compatibility. GE and SE multislice pulse sequences were used on an Oxford 2.0-T horizontal magnet, with clear bore diameter of 31 cm, equipped with Acustar S-180 gradients of 18-cm bore diameter, driven to 70 mT/m, using a Varian Unity Inova imaging platform. A group of images of the whole assembly and of its individual parts were obtained to detect image artifacts.

After identifying those materials causing significant distortion on the acquired images, the electrode was redesigned using MR-compatible materials, maintaining or improving the characteristics of the standard chronic assembly such as size, weight, and cost. In particular, after testing multiple commercially available connectors, the Omnetics Nano connector, normally used on the standard chronic assembly, was substituted with a zero insertion force (ZIF) Hirose connector, and the aluminum ring was eliminated. Although the selected connector is ideal for MRI applications, it has a very limited lifespan of only 10 connection/disconnection cycles [58], compared to 500 of the Omnetics Nano connector [59], limiting its use to acute or short term chronic studies. A flexible circuit was designed and fabricated to interconnect the new chronic probe with the acute headstage of data acquisition systems, used for neurophysiological applications, such as Plexon, Neuralynx, or Tucker Davis Technology (TDT) equipment. After that, both types of electrodes, the S−SiμE and the MR compatible silicon microelectrode (MRC−SiμE), were tested to evaluate displacement, torque, susceptibility artifacts, and possible heating as described in the following sections. Examples of the new designed electrode, as well as the flexible circuit, are shown in Fig. 2.

B. Translational Force

Following the recommendations in [10], each type of microelectrode was suspended from a very thin polypropylene suture filament (PROLENE 6-0, ETHICON, INC) attached to the

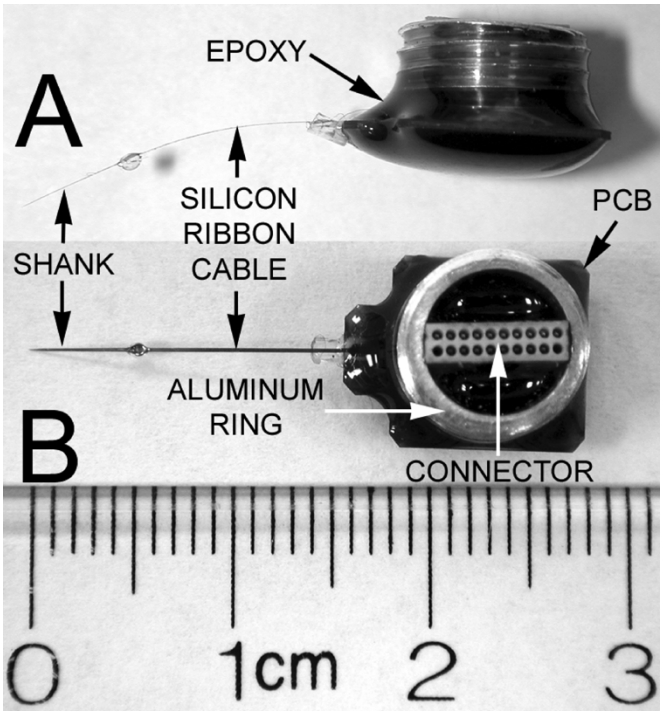

Fig. 1. (A) Side and (B) top view of a standard chronic assembly ($\mathrm{S-Si}\mu\mathrm{E}$) designed at the Center for Neural Communication Technology (CNCT) of the University of Michigan. The presented electrode is a single shank, 16-channel, recording electrode. The site spacing is 150 μm, the area of each site is approximately 170 $\mu\mathrm{m}^2$, the silicon ribbon cable has a length of 1 cm, and the shank is 5 mm long.

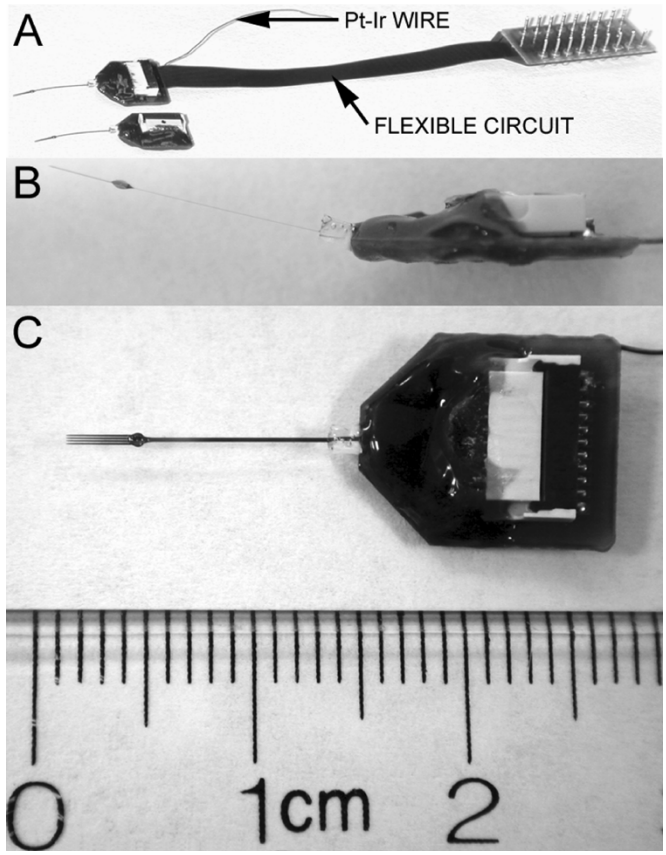

Fig. 2. (A) Flexible circuit to interconnect the MR compatible silicon microelectrode ($\mathrm{MRC-SI}\mu\mathrm{E}$) with data acquisition systems. The reference Pt-Ir wire (90%-10%), as the shown in the top assembly, is used for small animals and can be replaced with a metallic screw for large animals models. The flexible circuit can be connected inline with- or perpendicular to the electrode, depending on the application. (B) side and (C) top view of MR-compatible, 16-channel silicon microelectrode. The presented assembly is a four-shank, 4 channels per shank, recording electrode. The shank spacing is of 125 μm, the site spacing is of 100 μm, the site area is approximately 170 $\mu\mathrm{m}^2$, the silicon ribbon cable has a length of 1 cm, and the shanks are 3 mm long.

center indicator of a protractor. The weight of the filament was less than 1% the weight of each electrode assembly. The filament, holding the tested electrode, freely moved in a pendulum motion without touching the protractor at any place but the pivoting center. The zero mark position was obtained when the apparatus was very far from the 5-Gauss line and all angular measurements were taken when the apparatus was horizontally aligned, using a simple air-bubble level, and after the pendulum motion subsided. The test apparatus was positioned in different locations around the magnet so that the electrodes were placed at the point of maximum deflection, which, as expected, was near the opening of the bore. For each position, the angle α, defined as the maximum deflection of the device from the vertical direction to the nearest 1 °, was recorded. Finally, the ratio of the magnetic force F_M with respect the gravitational force, or weight of the device, was estimated, $\mathrm{F_M}/(\mathrm{m}\cdot\mathrm{g}) = \tan(\alpha)$, where m is the mass of the object and g is the acceleration due to gravity.

C. Rotational Force

Given the fragility and light weight of this type of electrodes and the observations made during the previous test, a more qualitative rotational force test than the recommended in [11] was performed. Using a small piece of adhesive tape, each microelectrode was attached to a light, thin, and rigid plastic dish. Then, the plastic piece, with the electrode in top of it, was placed at the surface of a container partially filled with water. The container was big enough to avoid restriction of movement of the floating dish and small enough to fit inside the magnet. Carefully, with slow movements, maintaining the piece under test away from the borders of the container, and keeping the whole assembly floating all the time, the water container was moved around the magnet and inside its bore in order to observe any rotation and alignment of the electrodes with respect to the main magnetic field.

D. MRI-Induced Heating

Given the high characteristic impedance of the silicon microelectrodes, which typically is around 1 $\mathrm{M}\Omega$ at 1 KHz and about 10 $\mathrm{K}\Omega$ for frequencies greater than 100 KHz [60], [61], and the small amount of metallic pieces used in them, significant MR-induced heating on these type of devices was not expected. Nevertheless, the heating test recommended in [41] was performed using a cost-effective temperature measurement system as suggested in [62]. Three temperature sensors (KT-210, TO-92 MINI, Infineon Technologies) provided calibrated resistive values proportional to the temperature, and their miniature plastic encapsulation and negligible power consumption, did not have a heating effect on the experiment. In addition, to

minimize electromagnetic inductions, twisted-shielded-pair cables of appropriate length were used and positioned at the symmetry axis of an eight-leg birdcage coil. The resistance measurements, acquired with three FLUKE multimeters placed outside the 5-Gauss line, were not affected by the RF signals. Each type of electrode was placed in a gelled phantom made with 0.8 g/L NaCl and 5.85 g/L Polyacrylic acid partial sodium salt (Sigma-Aldrich catalog number 436 364) in 0.5 L of distilled water [63]. This phantom simulates the electrical and thermal properties of human tissue and has been proven to be reliable for this type of test [64]. This setup represents an extreme condition where no heat dissipation occurs, other than conduction, because of the absence of convection or forced circulation of fluids, such as blood. For the $\mathrm{MRC}{-}\mathrm{Si}\mu\mathrm{E}$ the first sensor (S_1) was placed right at the tip of the electrode, the second one (S_2) as close as possible to the metallic contacts of the Hirose connector and the reference wire, and the last one (S_3) few centimeters away from the electrode, to sense the background temperature. For the $\mathrm{S}{-}\mathrm{Si}\mu\mathrm{E}$, S_1 and S_3 were placed in similar locations and S_2 in the space between the Omnetics connector and the aluminum ring.

After introducing the device under test into the bore of the magnet and waiting 20 min, to reach thermal equilibrium, the imaging session was performed using a multiecho-multislice, pulse sequence with the following imaging parameters: Field of view (FOV) of 12.8 cm $\times$ 12.8 cm, matrix size of 256 $\times$ 128 points, repetition time (TR) of 83.3 ms, echo time (TE) of 15 ms, number of averages (NAV) of 95, number of slices (NS) of 1, number of echoes (NE) of 4, and slice thickness (THK) of 2 cm. These parameters were selected not for imaging purposes but for having as many 180 ° RF pulses/s as possible and obtaining maximum gradient strength as fast as possible without causing self-heating of the scanner. The imaging time was almost 20 min, with a total of 57,344 180° RF pulses (48/s), and an estimated SAR of 1.14 W/kg for a 50-kg patient. The temperature readings from the three sensors were recorded every 30 s, starting and ending 5 min before and after the imaging session, and then 5 additional minutes after taking the phantom outside the MR scanner.

E. Image Artifacts

1) Microelectrodes: A plastic frame was built and used to hold the electrodes and to serve as a reference object in the MR images, as shown in Fig. 3. The $\mathrm{S}{-}\mathrm{Si}\mu\mathrm{E}$ was attached to the plastic frame using a small wooden rod and adhesive tape, whereas the $\mathrm{MRC}{-}\mathrm{Si}\mu\mathrm{E}$ was attached using adhesive tape and a section of the previously mentioned flexible circuit.

The plastic frame with the attached electrode was immersed into a container filled with distilled water doped with gadodiamide (Omniscan injection 287 mg/mL, 500 mM, Amersham Health) to reduce the T_1 relaxation to an estimated value of 300 ms. The Omniscan contrast agent was used instead of CuSO_4 recommended in [42] because the later reacted and damaged the aluminum ring of the $\mathrm{S}{-}\mathrm{Si}\mu\mathrm{E}$. Then, a group of sagittal SE and GE images were obtained with enough number of slices to span not only the whole electrode but also the distortion, if any, produced by it. All the images were acquired with the standard and swapped readout/phase-encode directions and the process

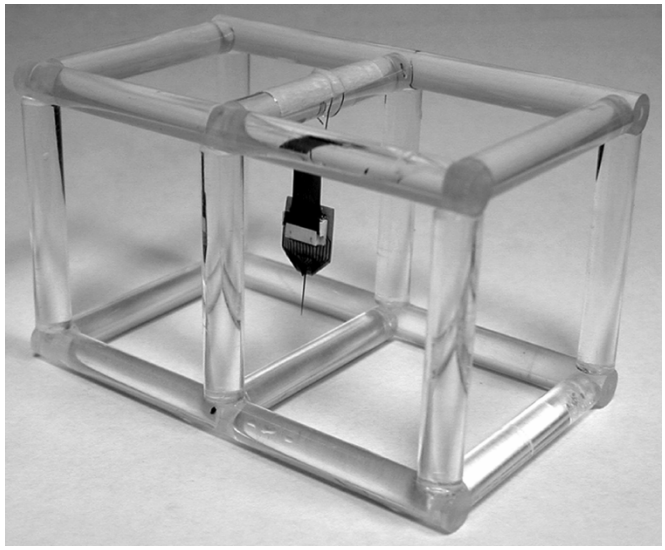

Fig. 3. MR-compatible frame used to hold the electrodes and to serve as a reference object in the MR image artifact test. Each rod of transparent acrylic had a diameter of 6.35 mm (1/4 in). The frame has a length of 8.5 cm, and approximately equal width and height of 5 cm.

was repeated with the electrodes in three different orthogonal positions with respect to the main magnetic field, and with the acquisition parameters shown in Figs. 6 and 7. The process was performed separately for the $\mathrm{S}{-}\mathrm{Si}\mu\mathrm{E}$ and the $\mathrm{MRC}{-}\mathrm{Si}\mu\mathrm{E}$ with the purpose of selecting the GE and SE images with the largest artifacts for each type of electrode.

2) Holding Screws: On the surgical procedure followed at the Neurophysiology Laboratory of the Kresge Hearing Research Institute (KHRI) at the University of Michigan, the $\mathrm{S}-\mathrm{Si}\mu\mathrm{E}$ is usually anchored at top of the skull of Guinea pigs using dental acrylic and stainless-steel screws (SS-316). In order to obtain the minimum image artifacts from the holding screw, which is also used as a reference electrode, not only this type of material was tested, but also titanium (Ti), polyetheretherketone (PEEK), and nylon (N) screws. Each one of them, approximately of the same dimensions, was fixed to a thin plastic sheet and inserted into a water phantom, which was then used to acquire GE images, with imaging parameters presented in Fig. 8.

F. Animal Testing

Four 16-channel $\mathrm{MRC}{-}\mathrm{Si}\mu\mathrm{E}$ were implanted in the auditory cortex of four Guinea pigs. The procedures followed an approved protocol, in compliance with guidelines set by the University of Michigan Committee on Use and Care of Animals, State and Federal regulations, and the standards of the Guide for the Care and Use of Laboratory Animals. Nylon screws were used in two animals and PEEK screws in another two. The probes were sterilized with ethylene oxide gas, and the screws using a steam autoclave. For the surgical procedure, which has been explained by Weiland and Vetter [60], [65], the animals were anesthetized with a 1:1 mixture of Ketamine:Xylazine whereas for the imaging session the animals were sedated using inhaled Isoflurane at 3% at a constant air flow of 1.5 L/min. The reference electrode was a Platinum-Iridium wire (Pt-Ir/90%-10%, A-M Systems, Inc.,

Catalog number 778 000) inserted into the neck of the animals. Pt-Ir was selected because this material presented much less artifacts on the images than the observed with titanium and stainless-steel screws, and it is a stable reference for short and long term neural recordings. After a short recovery period, the animals were imaged with the 2-T scanner using an eight-leg birdcage coil, a small surface coil, and a MR-compatible animal restrainer, all three of them purposely constructed to fit the Guinea pig head and the implanted microelectrodes.

Before and after imaging sessions, and in an anechoic chamber, electrophysiological signals driven by acoustic stimulation were recorded applying single tone, frequency sweep and broadband Gaussian noise stimuli. Furthermore, also before and after imaging sessions, the impedance of each electrode at 1 KHz was verified, for the 16 recording channels, to observe significant differences of this important characteristic of silicon microelectrodes.

III. Results

A. Initial Assessment

As observed in Fig. 4, the $\mathrm{S-Si}\mu\mathrm{E}$ produces a large image artifact that precludes any observation of the electrode and any possible tissue around it in a radius of about 1.5 cm. The detailed analysis of its parts revealed that the aluminum ring and mainly the Omnetics connector were the principal components producing the observed artifacts.

A direct MRI comparison between the Omnetics and the Hirose connectors, presented in Fig. 5, shows that, even though both connectors have similar dimensions, the shape of the Omnetics connector cannot be observed with MRI, whereas the Hirose connector produces a volume void that closely agrees with its dimensions.

B. Translational Force

The maximum displacement angle a of the $\mathrm{S-Si}\mu\mathrm{E}$ was of only 1 ° and therefore the magnetic force F_M, exerted over this electrode by the 2-T system, was not greater than 2% of the weight of the whole assembly. For the proposed $\mathrm{MRC-Si}\mu\mathrm{E}$, the result was even better, because no displacement angle was observed at all. Consequently, the magnetically induced translational force applied to this MR-compatible electrode at 2 T was negligible.

C. Rotational Force

The simple rotational force test performed, showed a very weak alignment of the $\mathrm{S-Si}\mu\mathrm{E}$ with the main magnetic field. The force was so weak that a small restriction of movement of the whole assembly was enough to stop the alignment and even redirect the electrode to any other arbitrary direction. The designed $\mathrm{MRC-Si}\mu\mathrm{E}$ did not show any rotation or alignment. In addition, no torque was observed holding each type of electrodes by hand while moving them inside the bore of the magnet.

D. MRI-Induced Heating

Neither the $\mathrm{S-Si}\mu\mathrm{E}$, nor the $\mathrm{MRC-Si}\mu\mathrm{E}$ presented any temperature increase under the mentioned conditions. All the temperature sensors remained within temperature oscillations below 0.4 °C, which is inside the accuracy of the measuring system. Note that the temperatures obtained from the $\mathrm{S-Si}\mu\mathrm{E}$, specifically from the sensor placed between the connector and the aluminum ring (S_2), were more noisy but still within the

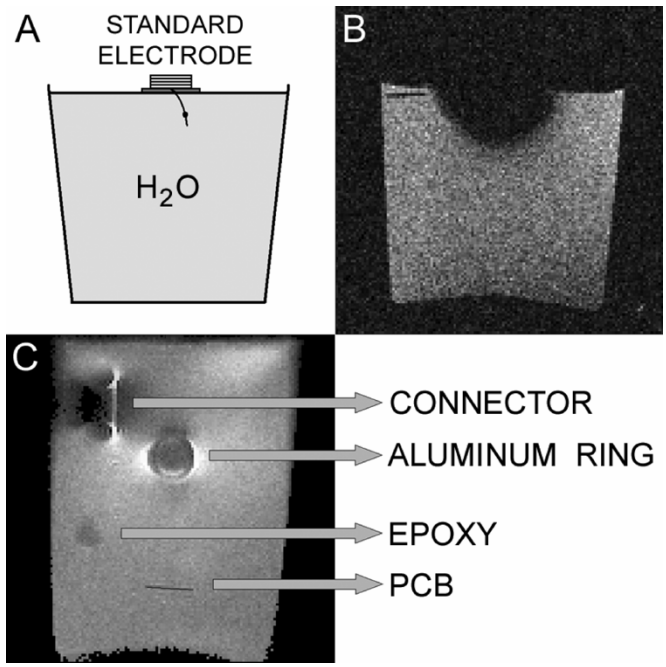

Fig. 4. MR test of standard chronic assembly. (A) The $\mathrm{S-Si}\mu\mathrm{E}$ was placed at the top of a glass of water. (B) GE images of the phantom were acquired with the following parameters: $\mathrm{FOV} = 6.4\ \mathrm{cm} \times 6.4\ \mathrm{cm}$, matrix of 128×128 points, $\mathrm{TR} = 7500\,\mathrm{ms}$, $\mathrm{TE} = 5\ \mathrm{ms}$, $\mathrm{NAV} = 1$, $\mathrm{NS} = 30$, $\mathrm{THK} = 1\,\mathrm{mm}$. Observe that the microelectrode produces an image distortion of about three centimeters in diameter, making impossible the observation of the silicon microelectrode and the surrounding areas. (C) Test of the individual components. All the parts were attached to a plastic film and immersed into a water phantom to obtain SE images with the following settings: $\mathrm{FOV} = 7.5\ \mathrm{cm} \times 7.5\ \mathrm{cm}$, 128×128 points, $\mathrm{TR} = 500\ \mathrm{ms}$, $\mathrm{TE} = 15\ \mathrm{ms}$, $\mathrm{NAV} = 4$, $\mathrm{NS} = 1$, and $\mathrm{THK} = 2\ \mathrm{mm}$. Observe that the Omnetic connector and the aluminum ring produce significant image intensity variations whereas the epoxy and the printed circuit board do not affect the images.

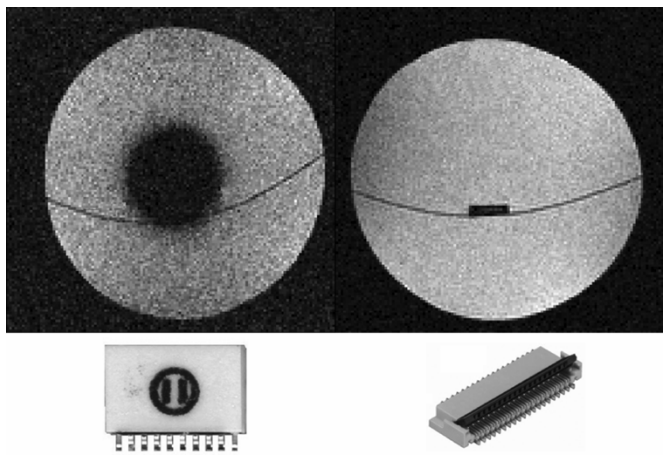

Fig. 5. GE images for MRI comparison between Omnetics (left) and Hirose (right) connectors. $\mathrm{FOV} = 6.4\ \mathrm{cm} \times 6.4\ \mathrm{cm}$, 128×128 points, $\mathrm{TR} = 7500\,\mathrm{ms}$, $\mathrm{TE} = 5\ \mathrm{ms}$, $\mathrm{NAV} = 1$, $\mathrm{NS} = 30/16$ (Omnetics/Hirose), $\mathrm{THK} = 1\ \mathrm{mm}$. Both connectors have approximate dimensions of $7\ \mathrm{mm} \times 4\ \mathrm{mm} \times 2\ \mathrm{mm}$. Observe that the Omnetics connector produces a large artifact whereas the Hirose connector presents a volume void that closely resembles its actual dimensions.

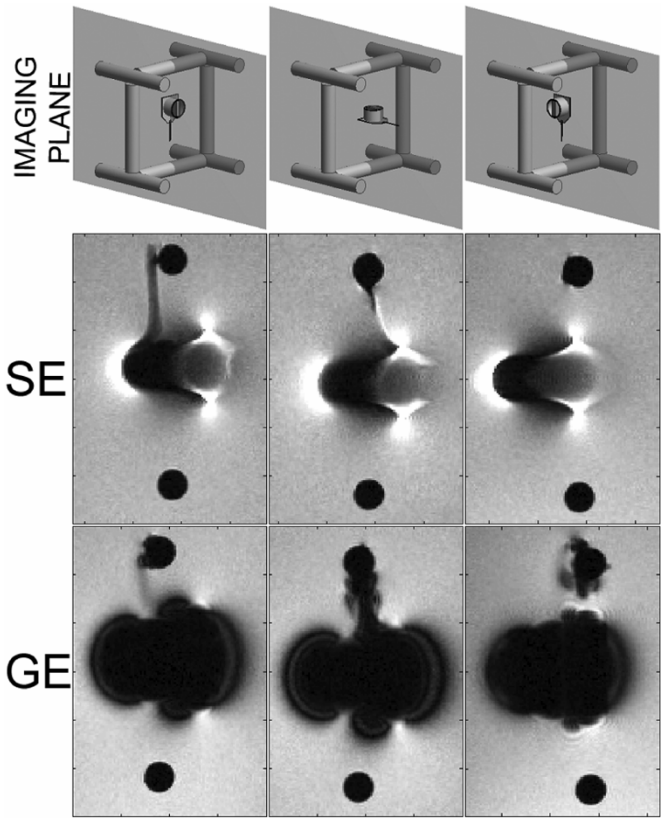

Fig. 6. Image artifact test for the S−SiμE. The top row indicates the imaging plane and the orientation of the electrode for each test, the middle row presents the worst images obtained using a SE pulse sequence, and the bottom row presents the worst images obtained with a GE pulse sequence. Each image covers an area of 6 cm × 4 cm, extracted from a FOV of 10 cm × 10 cm. The dark circles at the bottom and top of each image have a diameter of 0.635 cm, and indicate the position of the plastic frame orthogonal to the imaging plane. The imaging parameters were: Bandwidth $\mathrm{BW} = 32\ \mathrm{KHz}$, 256 × 256 points, $\mathrm{THK} = 3\ \mathrm{mm}$, $\mathrm{NAV} = 8$, $\mathrm{TR/TE} = 500/20\ \mathrm{ms}$ (SE) and 100/15 ms (GE), and flip angle of 30 ° (GE). Observe that the SE images present notorious intensity variations whereas the artifacts of the GE images cover larger areas.

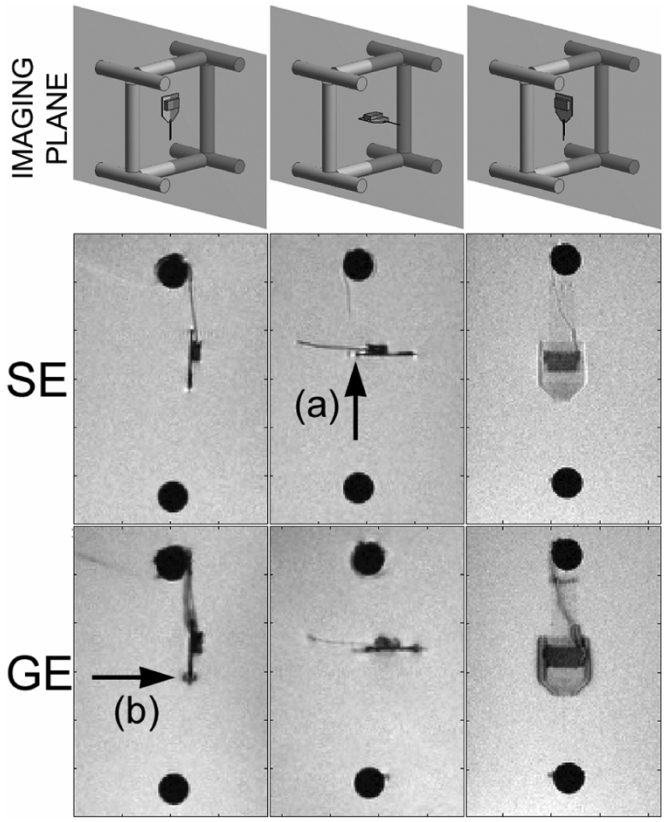

Fig. 7. Image artifact test for the MRC−SiμE. Similarly to the previous figure, the top row indicates the imaging plane and orientation of the electrode for each test, the middle row presents the worst images obtained using a SE pulse sequence and the bottom row presents the worst images obtained with a GE pulse sequence. The imaging parameters and size of the presented images are the same as the indicated in Fig. 6, and the same plastic frame was used for all the image artifact tests. Notice the similarity of the volume void produced by the electrode and the images observed in the SE and GE acquisitions, which closely resemble the actual shape of the electrode. Some minor distortions are observed at the soldering point of the reference Pt-Ir wire (a), and at the bonding wires (b), which normally are far enough from the silicon recording/stimulating sites.

mentioned range. Probably these noisy measurements were produced by current inductions in the metallic ring surrounding the sensor. Nevertheless, all the temperature measurements remained basically stable before, during, and after the RF and gradient switching excitation.

E. Image Artifacts

1) Microelectrodes: Figs. 6 and 7 present the result of the image artifact test for the S−SiμE and the MRC−SiμE respectively. As expected, the GE pulse sequence was more sensitive to magnetic susceptibility differences than the SE pulse sequence, because of the use of gradient refocusing instead of RF refocusing. As can be seen, the artifact produced by the S−SiμE affects the images such that the actual shape of the electrode and the surrounding regions are significantly distorted. Those areas would become useless for most or all MR-based imaging studies, unless the regions of interest (ROIs) were far enough of the implanted electrode. The artifact is evident, although different, in the SE and GE images; the first one presents the largest intensity variations, whereas the last one presents the largest affected regions.

The SE images of the MRC−SiμE present a volume void that closely corresponds to the actual shape of the tested microelectrode. The GE images show some minor signal variations in the regions of the metallic pins of the connector, in the soldering point of the Pt-Ir reference wire, and in the bonding contacts of the silicon microelectrode, although all of them no larger than a few millimeters. Noticeably, the silicon shanks of the electrode did not produce any distortion on any of the acquired images and they cannot be observed with the used imaging parameters.

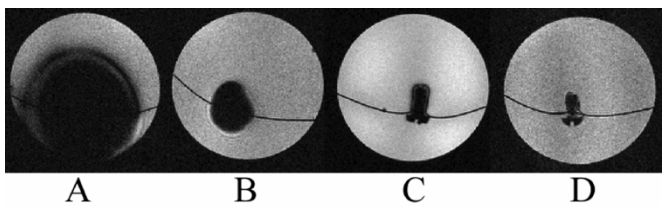

Fig. 8. MR test of holding screws. (A) Stainless-steel 316, (B) titanium, (C) PEEK, and (D) nylon screws fixed to a thin plastic sheet and inserted into a water phantom. GE images obtained with the following parameters: $\mathrm{FOV} = 5.12\ \mathrm{cm} \times 5.12\ \mathrm{cm}$, 256 × 256 points, $\mathrm{TR} = 50\ \mathrm{ms}$, $\mathrm{TE} = 15\ \mathrm{ms}$, and $\mathrm{THK} = 0.5\ \mathrm{mm}$.

2) Holding Screws: Fig. 8 presents a MR comparison of the tested holding screws. The image artifact created by the SS-316 screw [Fig. 8(A)] is so large that it even affects regions outside

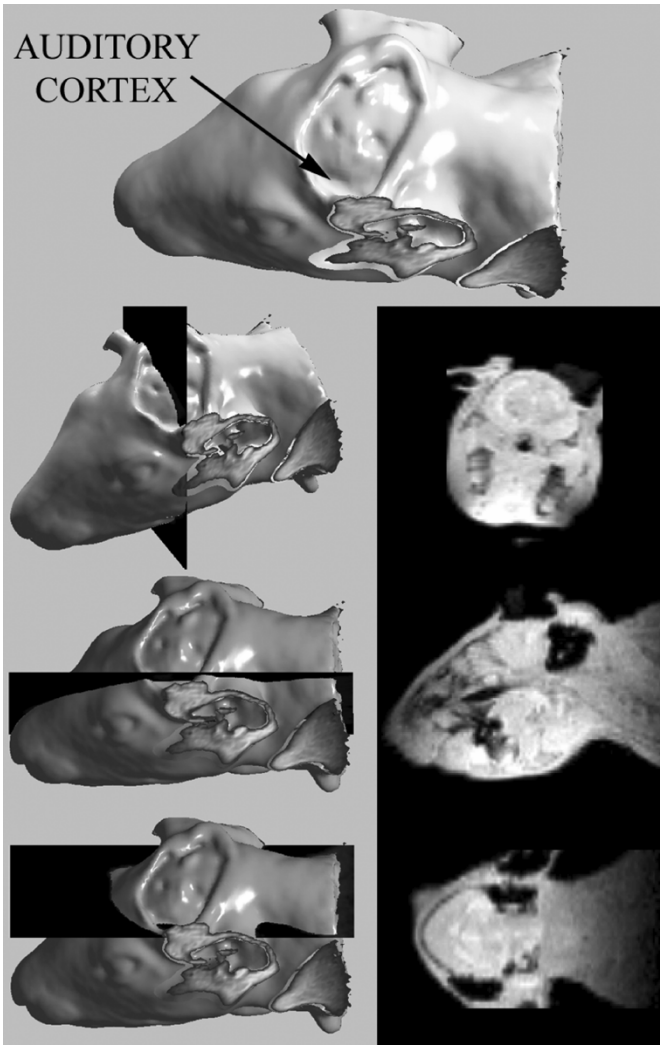

Fig. 9. Representative images and three-dimensional reconstructions of a Guinea pig head with an implanted MR compatible silicon microelectrode. The reconstructions and interpolated imaging planes were obtained using Matlab V6.5 (MathWorks), based on a GE multislice acquisition with the following parameters: $\mathrm{FOV} = 8\,\mathrm{cm} \times 8\,\mathrm{cm}$, 128×128 points, $\mathrm{TR} = 3\,\mathrm{s}$, $\mathrm{TE} = 3\,\mathrm{ms}$, $\mathrm{NAV} = 4$, $\mathrm{NS} = 36$, and $\mathrm{THK} = 1\,\mathrm{mm}$. Observe the area at the top of the head where the connector is installed and fixed using Nylon screws. The small depression in the brain, indicated with the arrow, indicates the place where the silicon microelectrode was implanted. All the imaging planes cross at the implantation site and no distortion is observed in any plane.

the used phantom. The image distortion from the Ti screw is smaller but large enough to hide the real shape of the screw [Fig. 8(B)]. Both images from plastic screws, Nylon and PEEK, present a volume void that strongly resembles the shape of the original pieces. The image of the Nylon screw presents a neat and clear shape [Fig. 8(D)] whereas the one from the PEEK screw appears slightly bigger than its actual shape [Fig. 8(C)]. We believe that either phantom vibration, metallic remnants of the machining process, or small air bubbles at the surface of the screw produced this effect. Previous reports present fully MR compatibility of both materials and therefore no image artifacts were expected [40], [43].

F. Animal Testing

In terms of image quality, electrophysiological signal recording, and impedance characteristic, the four animals performed equally well. As shown in Fig. 9, the images presented no distortion around the electrode and precisely delimited small indentation in the surface of the brain produced by the holding screws. The tissue at the top of the Guinea pig head is displaced because the electrode is mounted and anchored to the skull in that region. The auditory cortex, where the electrode was implanted, is also noticeable.

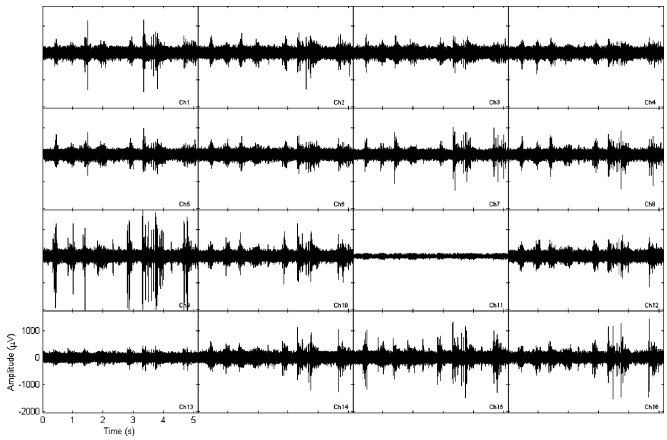

Fig. 10. Representative neural recordings obtained from the auditory cortex of a guinea pig using a 16-channel MR compatible chronic assembly. The neural activity was elicited using a 100 ms Gaussian noise burst with 2 stimuli/s.

The characteristic impedance of each electrode remained within normal values for the duration of the implants. In addition, the acoustically driven recorded brain signals were normal before and after imaging sessions, as those presented in Fig. 10, indicating that the intrinsic characteristics of the electrode were not affected and the electrode placement remained the same.

Unfortunately, the Nylon screws were not strong enough to hold the electrodes in place and the whole implant, electrode and dental acrylic, detached from the skull 1 and 2 weeks after implantation, for the two animals using this type of material. The PEEK screws performed exceedingly well in terms of mechanical stability and we have kept an animal for over nine months without any indication of implant damage or looseness. However, we noticed that the Hirose connector is easily affected by dirt particles that get into the metallic contacts. Therefore, for our more recent experiments, we are using a plastic cover, instead of the aluminum ring, to cover the electrode after implantation. The cover is a piece of a plastic vial specifically cut to protect the electrode and adjusted to the shape of the skull. It has a plastic lid that can be removed to connect a data acquisition system or closed to protect the connector during the daily life of the animal inside its cage.

IV. Discussion

Materials such as stainless-steel (nonmagnetic, austenitic, 300 Series), titanium, and other nonmagnetic metallic alloys, widely used for biomedical implants, do not represent significant risk of tissue damage in MR environments. Unfortunately, the amount of image artifact produced by the large susceptibility differences with respect to soft tissue makes the use of these materials particularly difficult in MRI applications. Other metals, such as platinum and tungsten, produce image artifacts that, in general, can be tolerated. On the other hand, nickel,

cobalt and iron, all of them ferromagnetic materials, are forbidden for MRI applications, mainly for safety reasons. In terms of image artifacts, they cannot be used unless the amount of material present in the imaging region is negligible with respect to the imaging volume. Nickel, in particular, is widely used in the electronic industry given its characteristics of hardness, corrosion resistance, and improved bonding of electroplated gold on metallic contacts. The minute amount of this material, used in most commercial connectors to increase their life span, causes significant image distortions in MR images. Used on connectors of neural implants, it makes the MR observation of these devices and the surrounding tissue virtually impossible. Although it produces small translational and rotational forces inside a MR scanner, with an appropriate fastening or holding procedure the risk of tissue damage can be easily minimized. In terms of image quality, if the ROI is sufficiently far away from the electrode, nickel plated connectors can be used in large animal models. For the case of iron, widely used in the lead frame of electronic integrated circuits in standard packages such as SOIC, DIP, TSSOP, etc., produces significant distortion on MR images and noticeable MR induced forces. Preliminary tests performed by the authors show that one way to avoid this problem on electronic devices is using integrated circuits without packaging, i.e., the die option, although it complicates the design of prototypes and significantly changes the design and fabrication of electronic systems.

The presented Hirose connector overcomes all the mentioned MR compatibility problems. Its tiny bronze and phosphor-bronze fitting and contacts respectively are very well suited for MR applications where not significant or small distortions are accepted. The lack of nickel and the construction of this type of connector highly improve the quality of the MR images but its life span is only 10 connection/disconnection cycles. Even though this life span is limited, this connector could be used without any problem in chronic experiments of relatively short duration, and for small or large animal models. In general, the mechanical characteristics of ZIF connectors limit their life span to 10 to 20 cycles even if they contain nickel [58]. Different methods to overcome this problem include the fabrication of a custom made Omnetics connector using tin electroplating instead of gold over nickel electroplating. Based on communications we had with the engineering group at Omnetics, this modification may increases the life span of the connector, perhaps to 100 or 200 cycles, but substantially increase the cost and the reliability is not warranted. Another solution is the use of the regular Omnetics Nano connector, or other small pitch connector, far enough from the imaging region by increasing the length of the flexible silicon ribbon cable or the Printed Circuit Board (PCB). While possible, this approach is limited to large animal models, makes more difficult the surgeries, and puts more stress in the yield factor of the fabrication process. We believe that the best solution is the removal of all connectors by designing an active probe with the required electronics to transmit the neuronal signals outside the magnet, by light or RF modulation, but certainly, more research and technological developments are still required to achieve this goal.

As mentioned earlier, in our studies, PEEK screws have shown excellent mechanical stability. In addition, several *in vivo* and *in vitro* studies present its biomedical compatibility characteristics [66]–[69]. In those studies, no tissue reaction, mutagenesis, or cell damage are observed, and even support of the growth and function of bone cells are reported. Absorption of only small quantities of protein structures from biological media, resistance to water, high temperature durability, good wear properties, chemical stability, and magnetic resonance compatibility, make PEEK a very good choice for biomedical implants and devices.

The presented research shows the magnetic resonance compatibility of a passive neural implant based on silicon technology. Extending that compatibility to an active biomedical implant, i.e., including all the devices required for neural recording or stimulation in the silicon probe, such as filters and amplifiers, is certainly required as well as challenging. Preliminary studies performed by the authors on commercially available systems, showed a noticeable rotation and displacement of the headstage and strong attraction of the preamplifier system. We believe that the use of active proves will improve the success of simultaneous electrophysiological recordings and MR imaging studies and minimize the problems observed with currently available commercial systems. For neural recordings, knowing that the sum of the bias current of the amplifiers typically used for this type of probe, and the ionic currents detected by the electrode are in the order of picoamperes and even femtoamperes, the expected forces due to circulating currents are negligible. For neural stimulation, given the characteristic high impedance of this type of electrodes, the stimulating current is limited by the compliance voltage of the current source. Normally, for the silicon microelectrodes, the current level for neural stimulation is well below 100 mA and therefore the expected displacement forces are also negligible [70]. The high impedance at both ends of the conductive ribbon cables, i.e., the silicon microelectrode in one end and the preamplifiers in the other, certainly would reduce the risk of MR-induced heating. In addition, the length of the cables could be easily adjusted to eliminate any resonant condition or changed to fiber optic. Special filters at the input of the amplifiers, to reduce RF signal rectification and therefore neuronal signal contamination, are certainly required.

Some advances have been reported using wire microelectrodes for simultaneous electrophysiological and fMRI BOLD signal recordings [51]. In general, some type of signal processing, magnet pulsing synchronization, and special electronic devices are necessary. In addition, some level of image distortion around the wire microelectrode is tolerated. Certainly, the advantages of silicon-based microelectrodes over wire or carbon fiber microelectrodes are so important, that additional efforts are required to make simultaneous multichannel neural recordings and fMRI BOLD signal acquisition a reality. Besides some obvious advantages, such as batch fabrication, channel density, high reproducibility, and precise dimensions, silicon based microelectrodes produce unnoticeable MR image distortions, compared to similar size wire or carbon fiber microelectrodes. This important difference makes the silicon technology the best choice for simultaneous electrophysiological and fMRI studies where the electrical activity of neurons can be better associated to brain activation detected with BOLD or other fMRI techniques, without causing significant MR

signal lose around the electrode, as those observed with other electrodes [51], [53]. Furthermore, the small MRI signature of silicon microelectrodes improves the quality of high-resolution anatomical images, and opens the possibilities for *in vitro* and *in vivo* studies of electrode localization, migration, and tissue reaction.

For chronic probes, tissue damage and reaction are subjects of current investigation. In general, all neural implants produce a response of the immune system that, over time, tends to mechanically and electrically isolate the electrode from the surrounding neuronal tissue. It is known that the electrode, the surgical procedure, the insertion and anchoring techniques, and the used animal species, among other factors, play an important role in the observed tissue reaction and electrode function after implantation [65], [71]. At a macroscopic level, we did not observe possible effects of MRI over the mentioned tissue damage and reaction, because we did not observe changes in the impedance of the electrodes and the characteristics of the recorded signals before and after imaging session. In addition, no image changes or artifacts were observed around the implanted electrodes over time. Certainly, in order to assess possible microscopic effects of MRI over the implanted microelectrodes that may affect the tissue, a more extensive study that includes histological analysis of control and MRI-tested sets of animals might be required.

V. Conclusion

We have presented a set of experiments and results demonstrating that the $\mathrm{S-Si}\mu\mathrm{E}$ and the $\mathrm{MRC-Si}\mu\mathrm{E}$ can be considered MR-safe and MR-compatible, respectively, for a cylindrical 2 T magnet and under the ASTM standards. Although an extensive study at higher magnetic fields was not performed for both electrodes, the authors have successfully tested the $\mathrm{MRC-Si}\mu\mathrm{E}$ at 3, 7 and 9.4 T research magnets without noticeable image distortions for conventional MRI protocols.

As can be seen, it is very important to design MR-compatible devices not only to avoid any risk to patients or animal subjects under study, but also to allow the use of MRI and fMRI to study the neurological responses induced by sensory stimuli or neural prostheses. Having MR compatible microelectrodes opens a new area of research where multichannel neuronal recordings can be complemented with simultaneous MRI/fMRI studies helping the scientific community to improve our understanding of the nervous system function. It is expected to increase research possibilities in many areas of the nervous system and even though the presented project is intended to be used on animals, it will create a solid base for future designs that will be used on humans.

Acknowledgment

The authors would like to thank all the people from the CNCT and KHRI, particularly J. Wiler, R. Oweiss, B. Casey, and J. Hetke.

References

[1] F. G. Shellock, *Magnetic Resonance Procedures: Health Effects and Safety*. Boca Raton, FL: CRC, 2001.

[2] US Food & Drug Administration. (2003, Jul.) Guidance for Industry and FDA Staff. Criteria for Significant Risk Investigations of Magnetic Resonance Diagnostic Devices. [Online]. Available: http://www.fda.gov/cdrh/ode/guidance/793.pdf

[3] A. Kangarlu and P.-M. L. Robitaille, "Biological effects and health implications in magnetic resonance imaging," *Concepts Magn. Reson.*, vol. 12, no. 5, pp. 321–359, 2000.

[4] A. M. Sawyer-Glover and F. G. Shellock, "Pre-MRI procedure screening: recommendations and safety considerations for biomedical implants and devices," *J. Magn. Reson. Imag.*, vol. 12, pp. 92–106, 2000.

[5] F. G. Shellock, "MR Imaging and electronically activated devices," *Radiology*, pp. 294–295, Apr. 2001.

[6] J. F. Schenck, "Safety of strong, static magnetic fields," *J. Magn. Reson. Imag.*, vol. 12, pp. 2–19, 2000.

[7] F. G. Shellock, J. A. Tkach, P. M. Ruggieri, and T. J. Masaryk, "Cardiac pacemakers, ICD's, and loop recorder: evaluation of translational attraction using conventional ("long-bore") and “short-bore" 1.5- and 3.0- Tesla MR systems," *J. Cardiovasc. Magn. Reson.*, vol. 5, no. 2, pp. 387–397, 2003.

[8] F. G. Shellock, "Magnetic resonance safety update 2002: implants and devices," *J. Magn. Reson. Imag.*, vol. 16, pp. 485–496, 2002.

[9] F. G. Shellock, J. A. Tkach, P. M. Ruggieri, T. J. Masaryk, and P. A. Rasmussen, "Aneurysm clips: evaluation of magnetic field interactions and translational attraction by use of “long-bore" and “short-bore" 3.0-T. MR imaging systems," *Am. J. Neuroradiol.*, vol. 24, pp. 463–471, Mar. 2003.

[10] American Society of Testing and Materials. (2002, Dec.) Standard Test Method for Measurement of Magnetically Induced Displacement Force on Medical Devices in the Magnetic Resonance Environment. [Online]. ASTM Designation: F 2052-02

[11] American Society of Testing and Materials. (2004, Feb.) Standard Test Method for Measurement of Magnetically Induced Torque on Medical Devices in the Magnetic Resonance Environment. [Online]. ASTM Designation: F 2213-04

[12] M. F. Dempsey, B. Condon, and D. M. Hadley, "Investigation of the factors responsible for burns during MRI," *J. Magn. Reson. Imag.*, vol. 13, pp. 627–631, 2001.

[13] W. R. Nitz, A. Oppelt, W. Renz, C. Manke, M. Lenhart, and J. Link, "On the heating of linear conductive structures as guide wires and catheters in interventional MRI," *J. Magn. Reson. Imag.*, vol. 13, pp. 105–114, 2001.

[14] J. Pictet, R. Meuli, S. Wicky, and J. J. van der Klink, "Radiofrequency heating effects around resonant lengths of wire in MRI," *Phys. Med. Biol.*, vol. 47, pp. 2973–2985, 2002.

[15] M. K. Konings, L. W. Bartels, H. F. M. Smits, and C. J. G. Bakker, "Heating around intravascular guidewires by resonating RF waves," *J. Magn. Reson. Imag.*, vol. 12, pp. 79–85, 2000.

[16] C.-Y. Liu, K. Farahani, D. S. K. Lu, G. Duckwiler, and A. Oppelt, "Safety of MRI-guided endovascular guidewire applications," *J. Magn. Reson. Imag.*, vol. 12, pp. 75–78, 2000.

[17] C. J. Yeung, R. C. Susil, and E. Atalar, "RF safety of wires in interventional MRI: using a safety index," *Magn. Reson. Med.*, vol. 47, pp. 187–193, 2002.

[18] C. J. Yeung, R. C. Susil, and E. Atalar, "RF heating due to conductive wires during MRI depends on the phase distribution of the transmit field," *Magn. Reson. Med.*, vol. 48, pp. 1096–1098, 2002.

[19] M. E. Ladd and H. H. Quick, "Reduction of resonant RF heating in intravascular catheters using coaxial chokes," *Magn. Reson. Med.*, vol. 43, pp. 615–619, 2000.

[20] C.-K. Chou, J. A. McDougall, and K. W. Chan, "RF heating of implanted spinal fusion stimulator during magnetic resonance imaging," *IEEE Trans. Biomed. Eng.*, vol. 44, no. 5, pp. 367–373, May 1997.

[21] H. Liu, W. A. Hall, A. J. Martin, and C. L. Truwit, "Biopsy needle tip artifact in MR-guided neurosurgery," *J. Magn. Reson. Imag.*, vol. 13, pp. 16–22, 2001.

[22] US Food & Drug Administration. (1998, Nov.) Guidance for the Submission of Premarket Notifications for Magnetic Resonance Diagnostic Devices. [Online]. Available: http://www.fda.gov/cdrh/ode/mri340.pdf

[23] L. Zaremba and R. Phillips, "FDA guidelines for magnetic resonance equipment safety," presented at the 44th American Association of Physicist in Medicine (AAPM) Annu. Meeting, Montreal, QC, Canada, Jul. 14–18, 2002.

[24] P. M. Colleti, "Size "H" oxygen cylinder: accidental MR projectile at 1.5 Tesla," *J. Magn. Reson. Imag.*, vol. 19, pp. 141–143, 2004.

[25] F. G. Shellock and E. Kanal, *Magnetic Resonance Bioefects, Safety, and Patient Management*, 2nd ed. Philadelphia, PA: Lippincott-Raven publishers, 1996.

[26] E. Kanal *et al.*, "American college of radiology white paper on MR safety," *Am. J. Roentgenol.*, vol. 178, pp. 1335–1347, Jun. 2002.

[27] Shellock R&D Services, Inc. and F. G. Shellock. (2004, Apr.) Your Information Resource for MRI Safety, Bioeffects, and Patient Management. [Online]. Available:http://www.mrisafety.com/

[28] Institute for Magnetic Resonance Safety, Education, and Research. (2004, Apr.). [Online]. Available: http://www.imrser.org/

[29] US Food & Drug Administration. (2001, Sep.) MRI Safety. [Online]. Available:http://www.fda.gov/cdrh/safety/mrisafety.html

[30] International Society for Magnetic Resonance in Medicine. (2004, Apr.) Spotlight on Patient Care & Safety. [Online]. Available: http://ismrm.org/

[31] E. Kanal. (2004, April) Magnetic Resonance Safety Site. Univ. Pittsburgh Medical Ctr.. [Online]. Available:http://www.radiology.upmc.edu/MRsafety/

[32] I. R. Young, "Notes on current safety issues in MRI," *NMR Biomed.*, vol. 13, pp. 109–115, 2000.

[33] B. A. Schueler *et al.*, "MRI compatibility and visibility assessment of implantable medical devices," *J. Magn. Reson. Imag.*, vol. 9, pp. 596–603, 1999.

[34] W. Greatbatch, V. Miller, and F. G. Shellock, "Magnetic resonance safety testing of a newly-developed fiber-optic cardiac pacing lead," *J. Magn. Reson. Imag.*, vol. 16, pp. 97–103, 2002.

[35] R. Obler, H. Köstler, B.-P. Weber, K. F. Mack, and H. Becker, "Safe electrical stimulation of the cochlear nerve at the promontory during functional magnetic resonance imaging," *Magn. Reson. Med.*, vol. 42, pp. 371–378, 1999.

[36] R. I. Goldman, J. M. Stern, J. Engel Jr., and M. S. Cohen, "Acquiring simultaneous EEG and functional MRI," *Clin. Neurophysiol.*, vol. 111, pp. 1974–1980, 2000.

[37] S. B. Baumann and D. C. Noll, "A modified electrode cap for EEG recordings in MRI scanners," *Clin. Neurophysiol.*, vol. 110, pp. 2189–2193, 1999.

[38] E. Hofmann, C. Preibisch, C. Knaus, J. Müller, C. Kremser, and C. Teissl, "Noninvasive direct stimulation of the cochlear nerve for functional MR imaging of the auditory cortex," *Am. J. Neuroradiol.*, vol. 20, pp. 1970–1972, Nov./Dec. 1999.

[39] A. C. S. Brau, C. T. Wheeler, L. W. Hedlund, and G. A. Johnson, "Fiber-optic stethoscope: a cardiac monitoring gating system for magnetic resonance microscopy," *Magn. Reson. Med.*, vol. 47, pp. 314–321, 2002.

[40] G. E. Medical Systems. (1997, Oct.) MR Safety and Compatibility: Test Guidelines for Signa SP (Version 1.0.). [Online]. Available:http://www.gemedicalsystems.com/rad/mri/products/spi/safety.html

[41] American Society of Testing and Materials. (2002, Dec.) Standard Test Method for Measurement of Radio Frequency Induced Heating Near Passive Implants During Magnetic Resonance Imaging. [Online]. ASTM Designation: F 2182-02

[42] American Society of Testing and Materials. (2001, Sep.) Standard Test Method for Evaluation of MR Image Artifacts From Passive Implants. [Online]. ASTM Designation: F 2119-01

[43] J. F. Schenck, "The role of magnetic susceptibility in magnetic resonance imaging: MRI magnetic compatibility of the first and second kinds," *Med. Phys.*, vol. 23, no. 6, pp. 815–850, 1996.

[44] E. M. Haacke, R. W. Brown, M. R. Thompson, and R. Venkatesan, *Magnetic Resonance Imaging. Physical Principles and Sequence Design*. New York: Wiley-Liss, 1999, ch. 25, p. 766.

[45] The University of Michigan Center for Neural Communication Technology. (2004, Jul.) Background on Silicon Substrate Probes. [Online]. Available: http://www.engin.umich.edu/center/cnct/

[46] K. D. Wise, D. J. Anderson, J. F. Hetke, D. R. Kipke, and K. Najafi, "Wireless implantable microsystems: high-density electronic interfaces to the nervous system," *Proc. IEEE*, vol. 92, no. 1, pp. 76–97, Jan. 2004.

[47] A. Standnes and CHEMIX. (2004, Apr.) School V2.81. Chemistry Software & Learning Tools for Chemistry. [Online]. Available: http://www.standnes.no/chemix/chemix.htm

[48] Reade Advanced Materials. (2004, Apr.) Magnetic Properties & Susceptibility Chart. [Online]. Available: http://www.reade.com/Particle_Briefings/magnetic_susceptibilities.html

[49] M. Winter, The University of Sheffield, and WebElements Ltd, UK.. (2004, Jul.) WebElementsTM, the Periodic Table on the WWW. [Online]. Available: http://www.webelements.com/

[50] K. Chinzei, R. Kikinis, and F. A. Jolesz, "MR compatibility of mechatronic devices: design criteria," in *Proc. 2nd Int. Conf. Medical Image Computing and Computer-Assisted Interventions*, Cambridge, U.K., Sep. 1999, pp. 1020–1031.

[51] N. K. Logothetis, J. Pauls, M. Augath, T. Trinath, and A. Oeltermann, "Neurophysiological investigation of the basis of the fMRI signal," *Nature*, vol. 412, pp. 150–157, 2001.

[52] S. H. Fung, D. Burstein, and R. T. Born, "*In vivo* microelectrode track reconstruction using magnetic resonance imaging," *J. Neurosci. Meth.*, vol. 80, pp. 215–224, 1998.

[53] B.-C. Shyu, C.-Y. Lin, J.-J. Sun, S.-L. Chen, and C. Chang, "BOLD response to direct thalamic stimulation reveals a functional connection between the medial thalamus and the anterior cingulate cortex in the rat," *Magn. Reson. Med.*, vol. 52, pp. 47–55, 2004.

[54] M. A. Howard III, I. O. Volkov, M. A. Granner, H. M. Damasio, M. C. Ollendieck, and H. E. Bakken, "A hybrid clinical-research depth electrode for acute and chronic *in vivo* microelectrode recording of human brain neurons," *J. Neurosurg.*, vol. 84, pp. 129–132, 1996.

[55] V. M. Tronnier, A. Staubert, S. Hähnel, and A. Sarem-Aslani, "Magnetic resonance imaging with implanted neurostimulators: an *in vitro* and *in vivo* study," *Neurosurgery*, vol. 44, pp. 118–125, 1999.

[56] G. Wang, M. W. Skinner, J. T. Rubinstein, M. A. Howard III, and M. W. Vannier, "Digital X-ray stereophotogrammetry for cochlear implants," *IEEE Trans. Biomed. Eng.*, vol. 47, no. 8, pp. 1120–1130, Aug. 2000.

[57] CNCT, "Passive Multichannel Recording and Stimulating Electrode Arrays. A Catalog of Available Designs," Univ. Michigan, Ctr. Neural Commun. Technol., Ann Arbor, MI, Mar. 1999.

[58] Hirose Electric Co., LTD.. (2005, Apr.) PCB-FPC/FFC Connectors. [Online]. Available: http://www.hirose-connectors.com/connectors-productcategory/fpcffcconnectors.htm

[59] Omnetics Connector Corporation. (2005, Apr.) E-Catalog. [Online]. Available: http://www.omnetics.com/ecatalog/OmneticsCatalog.pdf

[60] J. D. Weiland and D. J. Anderson, "Chronic neural stimulation with thin-film, iridium oxide electrodes," *IEEE Trans. Biomed. Eng.*, vol. 47, no. 7, pp. 911–918, Jul. 2000.

[61] J. D. Weiland, "Electrochemical properties of iridium oxide stimulating electrodes," Ph.D. dissertation, Dept. Biomed. Eng., Univ. Michigan, Ann Arbor, 1997.

[62] J. Häfner, M.-A. Golombeck, and O. Dössel, "Development of a cost-effective and MRI compatible temperature measurement system," *Biomedizinische Technik*, vol. 47-1, pp. 664–667, Sep. 2002.

[63] S. M. Park, J. A. Nyenhuis, C. D. Smith, E. J. Lim, K. S. Foster, and K. B. Baker *et al.*, "Gelled versus nongelled phantom materials for measurement of MRI-Induce temperature increases with bioimplants," *IEEE Trans. Magn.*, vol. 39, no. 5, pp. 3367–3371, Sep. 2003.

[64] A. R. Rezai, D. Finelli, J. A. Nyenhuis, G. Hrdlicka, J. Tkach, and A. Sharan *et al.*, "Neurostimulation systems for deep brain stimulation: *in vitro* evaluation of magnetic resonance imaging-related heating at 1.5 Tesla," *J. Magn. Reson. Imag.*, vol. 15, pp. 241–250, 2002.

[65] R. J. Vetter, J. C. Williams, J. F. Hetke, E. A. Nunamaker, and D. R. Kipke, "Chronic neural recording using silicon-substrate microelectrode arrays implanted in cerebral cortex," *IEEE Trans. Biomed. Eng.*, vol. 51, no. 6, pp. 896–904, Jun. 2004.

[66] M. S. Abu Bakar, M. H. W. Cheng, S. M. Tang, S. C. Yu, K. Liao, C. T. Tan, K. A. Khor, and P. Cheang, "Tensile properties, tension-tension fatigue and biological response of polyetheretherketone-hydroxypatite composites for load-bearing orthopedic implants," *Biomaterials*, vol. 24, pp. 2245–2250, 2003.

[67] A. Katzer, H. Marquardt, J. Westendorf, J. V. Wening, and G. von Foerster, "Polyetheretherketone—cytotoxicity and mutagenicity *in vitro*," *Biomaterials*, vol. 23, pp. 1749–1759, 2002.

[68] C.-H. Rivard, S. Rhalmi, and C. Coillard, "*In vivo* biocompatibility testing of PEEK polymer for a spinal implant system: a study in rabbits," *J. Biomed. Mater. Res.*, vol. 62, no. 4, pp. 488–498, Dec. 2002.

[69] T. W. Lin, A. A. Corvelli, C. G. Frondoza, J. C. Roberts, and D. S. Hungerford, "Glass PEEK composite promotes proliferation and osteocalcin production of human osteoblastic cells," *J. Biomed. Mater. Res.*, vol. 36, no. 2, pp. 137–144, 1997.

[70] A. W. Song and A. M. Takahashi, "Lorentz effect imaging," *Magn. Reson. Imag.*, vol. 19, pp. 763–767, 2001.

[71] D. H. Szarowski, M. D. Andersen, S. Retterer, A. J. Spence, M. Isaacson, H. G. Craighead, J. N. Turner, and W. Shain, "Brain responses to micromachined silicon devices," *Brain Res.*, vol. 983, pp. 23–35, 2003.

Francisco M. Martínez Santiesteban (M'04) was born in Durango, México. He received the engineering degree in electronics and communications from the Instituto Tecnológico y de Estudios Superiores de Monterrey (ITESM), Monterrey, Mexico, in 1989, and the M.S. in electronic engineering from the same institution in 1998 (both with the highest honors). He is currently working toward the Ph.D. degree in biomedical engineering at the University of Michigan, Ann Arbor.

He worked as an Automation Engineer, Electronic Maintenance Engineer, and Instrumentation Engineer from 1989 to 1995, developing instrumentation and control systems for different industries in Mexico. Since 1993, he has been involved in academia, as an Instructor and Lecturer for electronics, instrumentation, and medical imaging courses and laboratories at the ITESM and at the University of Michigan. His research interests include the design and fabrication of magnetic resonance compatible devices, and the simultaneous use of neural electrophysiological methods and functional MRI.

Mr. Martínez Santiesteban is student member of the International Society of Magnetic Resonance in Medicine, the Biomedical Engineering Society, and the Society for Neuroscience. He received the Fulbright/Garcia-Robles fellowship from 1999 to 2002, and the Encyclopedia Britannica grant in 1999 and 2000.

Scott D. Swanson received the B.S. degree in chemistry from the University of Michigan, Ann Arbor, in 1980 and the Ph.D. degree in physical chemistry from the University of Rochester, Rochester, NY, in 1990. His dissertation work, under the direction of Prof. R. Bryant, focused on the influence of water on polypeptide dynamics studies by solid-state NMR spectroscopy.

He is currently with the Department of Radiology, University of Michigan where he studies magnetization transfer between water and macromolecules and *in vivo* imaging of laser polarized xenon.

Dr. Swanson is a member of the International Society of Magnetic Resonance in Medicine where he has served on the scientific program committee.

Douglas C. Noll (M'83) received the M.S. and Ph.D. degrees in electrical engineering from Stanford University, Stanford, CA, in 1986 and 1991, respectively, and the B.S., degree, *summa cum laude*, in electrical engineering from Bucknell University, Lewisburg, PA, in 1985.

He is presently Professor of Biomedical Engineering and co-director of the Functional MRI Laboratory at the University of Michigan, Ann Arbor. From 1991–1998, he was Assistant and Associate Professor of Radiology and Bioengineering at the University of Pittsburgh. He has been performing research in magnetic resonance imaging (MRI) for over 16 years and has been active in research in functional MRI for 13 years. His recent work has focused on the acquisition, image reconstruction and processing methods for functional MRI and quantitative measurement and modeling of the physiological response to brain activity.

In 1994, Dr. Noll received the Isador I. Rabi Award from the International Society for Magnetic Resonance in Medicine (ISMRM) and was a member of the Board of Trustees of the ISMRM from 2000–2003. He is a member of the editorial board for *Magnetic Resonance in Medicine* and *Magnetic Resonance Imaging* and is a fellow of the American Institute of Medical and Biological Engineering.

David J. Anderson received the BSEE degree from Rensselaer Polytechnic Institute, Troy, NY, and the MS and Ph.D. degrees from the University of Wisconsin, Madison.

After completing a postdoctoral traineeship with the Laboratory of Neurophysiology, University of Wisconsin Medical School, he joined the University of Michigan, Ann Arbor, where he is now Professor of Electrical Engineering and Computer Science, Biomedical Engineering, and Otolaryngology. His research is in the areas of auditory physiology, neural recording device design and signal processing of neural recordings. He is the founding director of the University of Michigan Center for Neural Communication Technology, which conducts research on the development and use of silicon neural probe technology and distributes devices to neuroscientists worldwide.

Dr. Anderson is a fellow of the American Institute for Medical and Biological Engineering, a member of the Neuroscience Society, the Association for Research in Otolaryngology, and the Barany Society.